Active yet extremely durable Co3O4 spheroids of different texture without/with Au deposition for CO oxidation

Journal:	*Catalysis Science & Technology*
Manuscript ID:	CY-ART-08-2014-001054.R1
Article Type:	Paper
Date Submitted by the Author:	08-Oct-2014
Complete List of Authors:	Yao, Yao; Nanjing University, Su, Qin; Nanjing University, Feng, Xinzhen; Nanjing University, Bo, Sun; Nanjing University, Ji, Weijie; Nanjing University, Department of Chemistry Au, Chak-tong; Hong Kong Baptist University, Chemistry

Journal Name

RSCPublishing

ARTICLE

Active yet extremely durable Co_3O_4 spheroids of different texture without/with Au deposition for CO oxidation

Cite this: DOI: 10.1039/xoxxoooooox

Received ooth January 2012,
Accepted ooth January 2012

DOI: 10.1039/xoxxoooooox

www.rsc.org/

Y. Yao,[a,b] Q. Su,[a] X.Z. Feng,[a] B. Sun,[a] W.J. Ji, [a,b] * and C.T. Au [c] *

Spherically shaped Co_3O_4 particles were synthesized by one-pot solvothermal treatment of $Co(NO_3)_2$ in n-octanol free of structure directing agent or pore former. Au nanoparticles (2-4 nm) dispersed on the Co_3O_4 substrates were fabricated using deposition-precipitation method. The as-synthesized Co_3O_4 (without calcination) and the corresponding Au containing catalyst achieved complete CO oxidation at 90 °C and 80 °C, respectively. Upon calcination, the condensed Co_3O_4 formed on which uniform dispersion of small sized flat Au entities (3.0 ± 0.6 nm) with large Au-Co_3O_4 interfaces were established, showing complete CO oxidation at 110 °C. These two types of catalysts were found to be extremely durable even operated in a period beyond 70 h under certain conditions. The calcined Co_3O_4-based Au catalyst can outperform Au/d-Co_3O_4 in both activity and stability when subjected to a pre-reaction at 350°C for 5 h. The yolk-shell type Co_3O_4@SiO_2 catalysts synthesized by controllable acid-etching of Co_3O_4 cores demonstrated an optimal Co_3O_4 core-SiO_2 shell interaction and suitable Co_3O_4 core particle size for CO oxidation. Both Co_3O_4 substrates and Au/Co_3O_4 systems were found to encounter substantial activity enhancement by in-situ pretreatment. The pretreatment resulted in: (i) transformation of AuO_x to Au^0, (ii) higher fraction of surface Co^{3+}, and (iii) suitably lower concentration of surface oxygen adspecies, accounting for the enhanced activities.

Introduction

Low-temperature CO oxidation, perhaps the most extensively studied reaction in the history of heterogeneous catalysis, is becoming increasingly important in the context of cleaning air and lowering automotive emissions, as well as an important model catalysis reaction [1,2]. The noble metals of Pt and Rh were firstly found to be active for CO oxidation, however, these metals are very costly and their resources are also quite limited. According to the early observations reported by Hutchings et al. [3] and Haruta et al. [2,4-6], gold (Au) can exhibit high activity when deposited in nano-sized form on certain transition-metal oxides.

These findings motivated follow-up studies on different supported Au catalysts [7-8]. Many efforts have been devoted to explore other effective catalysts for CO oxidation. Among them, transition metal oxides have attracted great interest for the target reaction [9]. For instance, Wei et al. studied low temperature CO oxidation on the IB group metals and metal oxides [10]. Recently, Qian et al. studied the catalytically active structures of SiO_2-supported Au nanoparticles (NPs) for low-temperature CO oxidation. It was emphasized that not only the particle size but also the electronic property of Au NPs determined the CO oxidation activity [11]. Besides CO oxidation, the Au NPs highly dispersed on metal oxides were also found to be active for the reactions such as ozone decomposition, hydrogen oxidation, and CO + NO reaction [12-15]. It is generally recognized that preparation chemistry plays an important role in determining the Au-based catalysts [16-18]. On the other hand, the development of active yet stable catalysts without noble metals for CO oxidation under mild conditions still remains a challenge [2]. Among various metal oxides, cobalt oxide was reported to be active for CO as well as hydrocarbons oxidation [19-23]. It is known that the properties of materials with the same composition but different structure or morphologies can vary substantially [15,24,25]. Therefore, various morphologies of Co_3O_4 structures, such as Co_3O_4 nanobelts [26], nanosheets [27], nanowires [28], nanorods [3], and nanocubes [29], showed distinct morphological effect in CO oxidation. Co_3O_4 also showed morphology-dependent catalysis in certain reactions [2,26-29,30]. For instance, the Co_3O_4 entities of different morphology showed the following activity order for CH_4 combustion: nanosheets >

nanobelts > nanocubes [31]. The specifically exposed facets of a certain morphological nano-crystallite comprise the unique arrangement of surface cations and anions, which in turn build up active sites of different reactivity. Featuring the hollow interior surfaces and high surface/volume ratio, the Co_3O_4 nanotubes were synthesized by Bae et al. [32]. The synthesis of Co_3O_4 nanotubes through Kirkendall effect has been recently reported by us, and the obtained material showed excellent activity and good stability toward the catalytic combustion of CH_4 [33]. The Co_3O_4-based materials exhibited a reaction-induced activity enhancement for CO oxidation even if the Au NPs are absent. This observation is remarkably different from that on the hollow structured Au/FeO_x nanostructures recently reported by us [34].

In recent years, the core-shell type materials have been widely studied for their unique chemical and physical properties and potential applications in different areas [35]. High activity and/or unique selectivity of core-shell nanostructures can be obtained by fine-tuning the size and shape of cores as well as the composition and thickness of shells [36]. The protective shells can effectively avoid the small-sized core particles from sintering especially when the reactions were operated at high temperatures [37]. Compared to the microporous silica shells, the mesoporous silica shells encapsulated the Fe, Ni, and Ru cores showing superior activities for ammonia decomposition [37b-d], methane partial oxidation to syngas [37e,f], and CO oxidation [37g]. Deng et al. employed a surfactant-templating approach to fabricating the magnetite core and the ordered mesoporous silica shell with perpendicularly oriented channels [38]. For the yolk-shell type catalyst, the structural configuration can provide a unique reaction environment, which can function as a micro capsular-like reactor in some circumstances [37e,39].

In the present study we synthesized the Co_3O_4 based catalysts (with/without Au deposition) for CO oxidation. The major concern is catalyst durability. We fabricated the Co_3O_4 bases of spherical morphology through an easy solovthermal treatment of $Co(NO_3)_2$. Upon different thermal treatment (drying/calcination), we were able to modify the texture/porosity of Co_3O_4 base, and further the Au-Co_3O_4 interaction, which would in turn dramatically influence catalyst stability for the target reaction. We also fabricated the Co_3O_4 based catalysts by isolating the Co_3O_4 particles with SiO_2 layer and further tuned the Co_3O_4 particle size by acid etching of the derived core-shell type catalysts. The employed preparation strategies enable us to have developed the Co_3O_4 based catalysts (with/without Au deposition) showing significantly different catalyst stability and activity. We also learned the originality of catalyst behaviors from the detailed characterizations, which was proved not to be limited to the Co^{3+} content in the samples.

Experimental

Preparation of catalysts

Spherical Co_3O_4 particles: $Co(NO_3)_2{\cdot}6H_2O$ (1.4 g) was dissolved in *n*-octanol (100 ml) to make a solution, then the temperature was increased to 180 °C and kept at this temperature for 4 h. After that the material was collected by centrifugation, washed three times with distilled water, and dried under an IR-lamp. The dried sample was denoted as d-Co_3O_4. If the dried sample was further calcined in air at 500 °C for 3 h, the calcined sample was denoted as c-Co_3O_4.

Au/Co_3O_4: the deposition-precipitation method was employed to prepare the Au/Co_3O_4 samples. In the case of Au/d-Co_3O_4, certain amount of d-Co_3O_4 was dispersed in a mixture of distilled water and ethanol (10:1, v/v), and the use of ethanol is helpful to achieve uniform dispersion of d-Co_3O_4 in the suspension. The $HAuCl_4{\cdot}3H_2O$ solution (0.01 M) was then added, giving the nominal Au loading is 3% by weight. In the case of Au/c-Co_3O_4, certain amount of c-Co_3O_4 was dispersed in distilled water (30 ml). The ammonium solution (0.07 mol/L) was added to the preparation media until the pH value of 9 was reached for preparing both Au/d-Co_3O_4 and Au/c-Co_3O_4. After that, the slurry was put into a water bath (at 50 °C) and magnetically stirred for 2 h. The solids were collected by repeated centrifugation and washing with distilled water (twice) and ethanol (one time). They were dried at room temperature (RT) overnight. The Au content of Au/d-Co_3O_4 and Au/c-Co_3O_4 is 1.9 wt% and 2.1 wt% respectively according to the ICP-AES measurement.

Co_3O_4@SiO_2: certain amount of Co_3O_4 particles (d- and c-Co_3O_4) was first dispersed in a mixture of distilled water (30 ml) and ethanol (10 ml), after that ammonium hydroxide (2 ml) was added under sonication in an ultrasound cleaner (KQ-100DE, 40 kHz, 100 W). Then TEOS (the Si/Co atomic ratio =1/2) was injected into the suspension by a microsyringe under sonication. One hour later, the materials were collected by centrifugation, washed three times by distilled water and dried at 100°C.

Acid-etched Co_3O_4@SiO_2: The Co_3O_4@SiO_2 particles (1 g) was put into a mixture containing HNO_3 (20 ml, 5 mol/L) and distilled water (10 ml) and magnetically stirred for 30 min. The slurry was put into a water bath (at 50 °C) and the suspension was continuously stirred for 5 h. The solids were collected by centrifugation, washed with distilled water, and dried at 80 °C overnight.

Materials characterization

X-ray diffraction (XRD) measurement was conducted on a Philips X'Pert MPD Pro X-ray diffractometer with Cu Kα radiation (λ = 0.1541 nm). The TEM images were taken over a JEOL JEM-1010 microscopy operated at 100 kV. The HRTEM images were taken on a JEOL JEM-2010 microscopy operated at 200 kV. N_2 sorption measurement was performed on a NOVA-2020 Material Physical Structure Determinator. Before measurement, sample was degassed at 300 °C for 3 h. BET surface areas were calculated based on a multipoint BET analysis of the nitrogen adsorption isotherms. Oxygen temperature-programmed desorption (O_2-TPD) was carried out

using a U-shaped quartz reactor. The catalyst (100 mg) was first pretreated in a He stream at 120 °C for 1 h, and then oxygen adsorption proceeded by exposure to pure O_2 at RT for 0.5 h. The sample was purged in a He flow (60 ml min^{-1}) for 1 h and then heated to 600 °C at a rate of 10 °C min^{-1} in a He flow (60 ml min^{-1}), and the effluent gas was analyzed using a thermal conductivity detector (TCD). Hydrogen temperature-programmed reduction (H_2-TPR) was performed using the same system as in O_2-TPD. The sample (100 mg) was purged in a He flow (50 ml min^{-1}) for 1 h and then heated to 700 °C at a rate of 10 °C min^{-1} in a 5%H_2-Ar flow (50 ml min^{-1}), and the effluent gas was analyzed using a TCD. X-ray photoelectron spectroscopy (XPS) analysis was performed on a PHI 5000 Versaprobe system, using monochromatic Al Kα radiation (1486.6 eV) operating at 25 W. The sample was outgassed overnight at RT in a UHV chamber (< 5×10^{-7} Pa). All binding energies (BEs) were referenced to the C1s peak at 284.6 eV. TG analysis was operated on NETZSCH STA 449C (Germany). The sample of ca. 100 mg was first purged in an Ar flow (50 ml min^{-1}) at 100°C for 1 h and then cooled down to RT. After that, the sample was heated to 450 °C at a rate of 5 °C min^{-1} in a 5%H_2-Ar flow (50 ml min^{-1}) meanwhile the weight loss was recorded.

Catalyst activity

Catalyst of 50 mg was placed into a quartz tube reactor and evaluated in CO oxidation operated at atmospheric pressure. The feed gas (1.6% CO, 21.0% O_2, and balanced N_2) was passed through the catalyst bed at a total flow rate of 25 ml min^{-1}, giving a corresponding gas hourly space velocity (GHSV) of 30,000 ml g_{cat}^{-1} h^{-1}. In some cases, the catalysts were first pretreated in a flow of reaction feed at 180 °C for 120 min. The inlet and outlet gas compositions were analyzed online using a gas chromatograph (GC-122). The TORs were calculated on the basis of unit surface area of samples. Both the Co_3O_4 substrates and the Au species were found to be comparably active for the reaction, the TORs were thus estimated based on the total surface areas of samples rather than that of Co_3O_4 or Au individual, which were determined by physisorption of N_2 at low temperature (BET).

Results and discussion

TEM/XRD

The mono-dispersed and spherically shaped Co_3O_4 particles with diameters of ca. 170-200 nm can be obtained by employing $Co(NO_3)_2{\cdot}6H_2O$ and *n*-octanol as the raw materials upon solovthermal treatment without PVP addition [40]. For the d-Co_3O_4 particles without calcination, it is clearly evident that there are rich of fine pores inside the bulk phase, yielding a highly loose sample texture (Fig. 1a). Upon 500 °C-calcination of d-Co_3O_4 spheroids, some hollow structures are evidently developed inside the spheroids meanwhile the sample texture became highly condensed (Fig. 1b), resulting from the shrinkage of structurally loose d-Co_3O_4 spheroids upon high temperature calcination, which was further confirmed by the following N_2 sorption measurement.

In case PVP was employed, the morphological and textural properties of the resulting Co_3O_4 particles could be notably modified: Xie et al. [2] reported that the adsorption of PVP onto the Co_3O_4 particle surface via the hydrogen bonding stabilized the Co_3O_4 entities and prevent them from agglomeration under the employed solvothermal conditions. In case the d-Co_3O_4 spheroids were used as support, extremely fine Au NPs (< 2 nm) could be confined in the micropores of d-Co_3O_4 (Fig. 1a), while if the c-Co_3O_4 spheroids were applied, the Au NPs were found to be uniformly distributed on the condensed surfaces of the Co_3O_4 spheroids. Note also that the Au NPs deposited on the surfaces of c-Co_3O_4 spheroids showed rather flat particle morphology (Fig. 1b), with the mean particle size of 3.0 ± 0.6 nm (Fig. 2a). HRTEM analysis was conducted on Au/c-Co_3O_4 (used) to take a close view of Au-Co_3O_4 interface. The trapezoidal Au entity with a ratio of height to basement width being about 2 and the hemispheric Au entity with the largest basement area can be figured out from the HRTEM images (Fig. S1). In both cases, large Au-Co_3O_4 interfaces were developed, and in the case of trapezoidal Au entity, change in Au atoms arrangement (from oblique rows to nearly vertical ones with respect to substrate) at the Au-Co_3O_4 boundary can also be figured out. Such structural variation is thought to be the result of the most favourable and intensive Au-Co_3O_4 interaction.

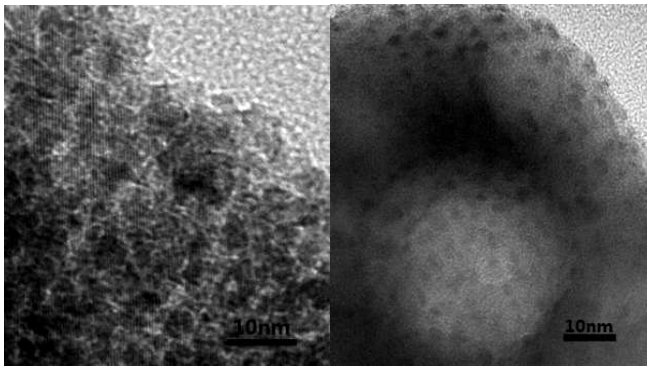

(a) (b)

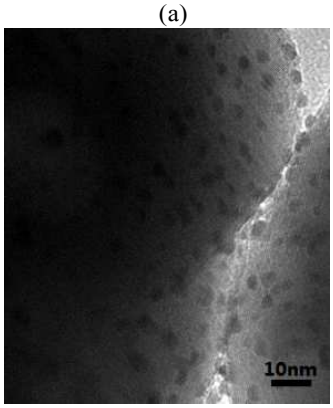

(c)

Fig. 1 TEM images of (a) Au/d-Co_3O_4, (b) Au/c-Co_3O_4, (c) used Au/c-Co_3O_4.

It is commonly recognized that Au NPs easily suffer from a significant activity drop upon high-temperature calcination and/or reaction [8]. This situation may adversely influence the application of Au NPs when the operation and regeneration of catalysts at elevated temperature are needed [41]. In the present case, the mean particle size of the Au NPs on the c-Co_3O_4 spheroids only slightly changed (4.2 ± 0.8 nm, Fig. 2b) even subjected to a reaction period > 70 h. It is deduced that there is strong interaction between the Au NPs and the condensed surfaces of the calcined Co_3O_4 spheroids, which in turn effectively stabilized the small-sized Au NPs during the reaction. In this study, the core-shell structured Au/Co_3O_4@SiO_2 was also fabricated by coating a silica layer of approximately 10 nm in thickness onto the Au/Co_3O_4 system (Fig. 1d).

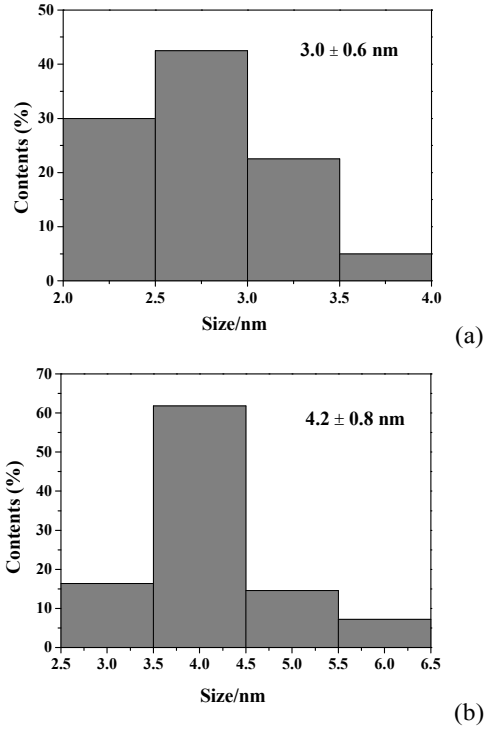

Fig. 2 Au particle size distribution in (a) Au/c-Co_3O_4 and (b) used Au/c-Co_3O_4 (> 70 h reaction).

In addition, the core-shell structures of Co_3O_4@SiO_2 (without Au deposition) with tunable size of Co_3O_4 cores were fabricated by the controlled acid-etching process (Fig. 3). Employing different acid-etching temperature and period, the size of Co_3O_4 cores can be systematically tuned; generating the internal cavities of different sizes in the resulting core-shell structures. These are the first examples of the Co_3O_4-based catalysts with the unique core-shell structural features for CO oxidation.

According to the XRD patterns of various samples shown in Fig. 4, only the Co_3O_4 phase structure can be identified even for the d-Co_3O_4 (JCPDS 42-1467) [42]. The d-Co_3O_4 based samples, whether containing Au NPs or not, showed relatively low peak intensities, indicating comparably lower sample crystallinities. This is consistent with the TEM observations. There is no signal attributable to the Au component, suggesting high dispersion of very fine Au entities on the substrates of both d-Co_3O_4 and c-Co_3O_4, as previously revealed by the TEM images (Figs. 1a-c).

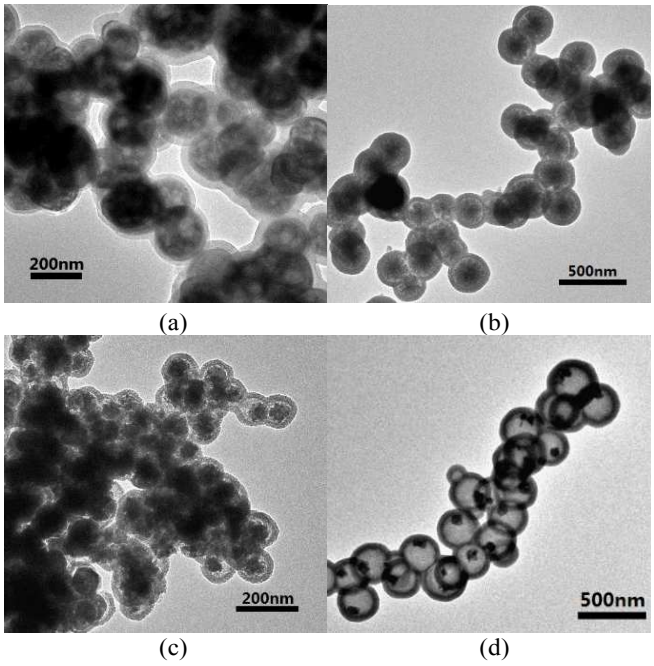

Fig. 3 TEM images: (a) non-acid-etched Co_3O_4@SiO_2, (b) slightly acid-etched Co_3O_4@SiO_2, (c) moderatly acid-etched Co_3O_4@SiO_2, and (d) heavily acid-etched Co_3O_4@SiO_2.

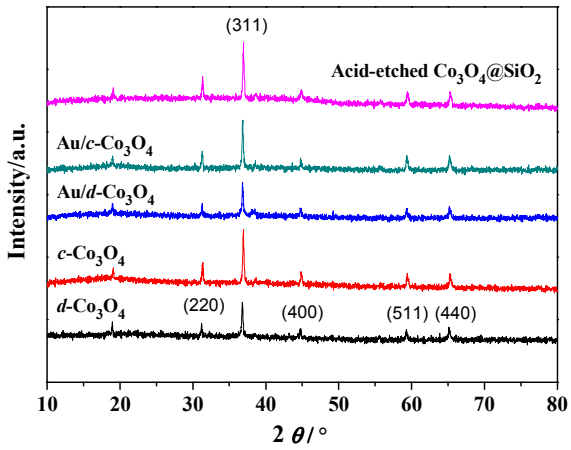

Fig. 4 XRD patterns of various Co_3O_4-based catalysts.

N_2 sorption measurement

Based on the N_2 sorption measurements of the d-Co_3O_4, c-Co_3O_4, Au/d-Co_3O_4, and Au/c-Co_3O_4, the BET surface areas of samples and the adsorption-desorption isotherms are presented in Table 1 and Fig. 5, respectively. The BET surface area of d-Co_3O_4 and Au/d-Co_3O_4 is 215.6 and 127.1 m^2/g respectively. Note that the value of c-Co_3O_4 and Au/c-Co_3O_4 was 8.5 and 12.3 m^2 g^{-1} respectively. Not only surface areas but also pore volumes dramatically decreased on the c-Co_3O_4 and Au/c-Co_3O_4 samples. Upon thermal treatment, the structurally loose d-Co_3O_4 substrate (also in Au/d-Co_3O_4) would transformed into more structurally dense c-Co_3O_4, accompanying structure shrinkage, loss of abundant micro-porosity, and creation of inaccessible internal hollows. These dramatic structural variations upon calcination significantly reduced the surface area of d-Co_3O_4 and Au/d-Co_3O_4 and eliminated most of the pore volume mainly existing in d-Co_3O_4 substrate (Table 1). Au presence in the micropores of d-Co_3O_4 substrate likely blocked some fine pores, leading to decrease in pore volume and also apparent shift of pore size. The surface area of c-Co_3O_4 was increased from 8.5 to 12.3 m^2 g^{-1} after Au addition, mainly attributable to the presence of Au entities. Note that pore volume of c-Co_3O_4 changed insignificantly (from 0.02 to 0.03 cm^3 g^{-1}), and this minor increment in pore volume could be due to the result of slight dissolution of c-Co_3O_4 in the acidic $HAuCl_4$ medium. The results of N_2 sorption measurements are coincident well with the TEM observations (Fig. 1).

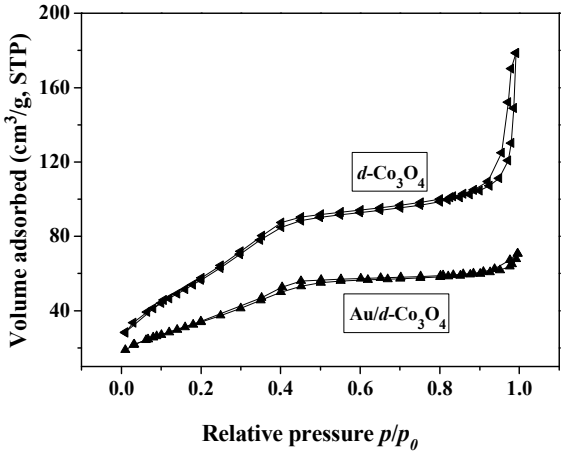

(a)

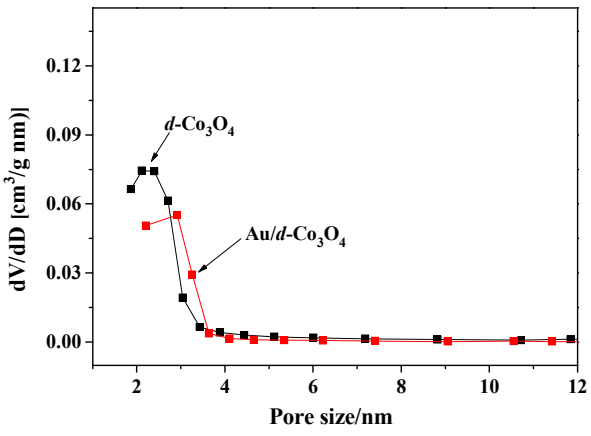

(b)

Fig. 5 (a) Nitrogen adsorption-desorption isotherms and (b) pore size distribution of d-Co_3O_4 and Au/d-Co_3O_4.

There are type II and V isotherms with inconspicuous hysteresis loops for d-Co_3O_4 and Au/d-Co_3O_4, (Fig. 5a), suggesting the presence of nonlinear mesopores in the samples. The pore size distributions (Fig. 5b) calculated by the Barrett-Joyner-Halenda (BJH) method based on the desorption branches of the isotherms demonstrated that the average pore diameter of the corresponding samples are in the range of 2.5-3 nm.

Table 1 BET surface areas and pore volumes of d-Co_3O_4, c-Co_3O_4, Au/d-Co_3O_4, Au/c-Co_3O_4, and Co_3O_4@SiO_2 (calcined)

Catalyst	BET surface area (m^2 g^{-1})	Pore volume (cm^3 g^{-1})
d-Co_3O_4	215.6	0.18
c-Co_3O_4	8.5	0.02
Au/*d*-Co_3O_4	127.1	0.09
Au/*c*-Co_3O_4	12.3	0.03
Co_3O_4@SiO_2 (calcined)	276.3	0.16

O_2-TPD/H_2-TPR/TGA

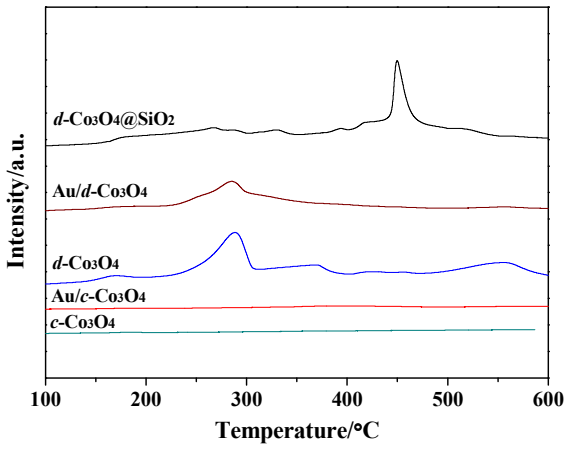

Fig.e 6 O_2-TPD profiles of the d-Co_3O_4 and c-Co_3O_4 based catalysts with and without Au NPs.

In order to better understand the nature of the Co_3O_4 substrates (with and without calcination) as well as the Au-containing catalysts in CO oxidation, the O_2-TPD technique was employed to investigate the oxygen adsorption/desorption behaviors over these catalysts, and the results are shown in Fig. 6. The desorption peak below 350 °C can be ascribed to the desorption of weakly adsorbed oxygen species such as O_2^- and O^-, while the one above 400 °C can be attributed to the desorption of the lattice oxygen species [43]. The molecularly adsorbed oxygen $O_{2\,(ad)}$ and the $O_{2\,(ad)}^-$ and $O_{(ad)}^-$ ones are weakly bonded to substrate surface, while the $O_{(lattice)}^{2-}$ species is usually thought to be a kind of surface lattice oxygen, and is difficult to remove. In general, the greater amount of surface oxygen species exists (corresponding to the desorption peaks in the 150-350 °C

range), the higher the catalytic ability for oxidation reaction will be [15]. According to Fig. 6, the type and amount of oxygen adspecies change with sample constitution and preparation history. There was higher concentration of surface oxygen adspecies on the d-Co_3O_4 substrate as compared to the c-Co_3O_4 counterpart, due to the fact that the former had much greater specific surface area than the latter. When Au NPs were deposited onto the Co_3O_4 substrate, the density of surface oxygen adspecies apparently decreased. Similar observation was made on the hollow structured Au/FeO_x [34] and further demonstrated by XPS investigation (see below). With silica encapsulation of Co_3O_4, the amount of surface oxygen adspecies also decreased (in the 150-350 °C range), suggesting there should be strong interaction between the Co_3O_4 cores and the SiO_2 shells. Such core-shell interaction could restrain oxygen adsorption on the core surfaces, which in turn affected the catalytic behavior of the core-shell type catalyst. Note that there were additional desorption peaks in the 400-500 °C range over the core-shell catalyst, probably attributable to the presence of SiO_2 shells. In view of the higher desorption temperatures, the associated species would be less reactive for CO oxidation.

H_2-TPR and TG analysis under reducing atmosphere were conducted over d-Co_3O_4, c-Co_3O_4, Au/d-Co_3O_4, and Au/c-Co_3O_4. The temperature range for removal of adsorbed oxygen species and lattice oxygen species associated with Co^{3+} and Co^{2+} can be figured out in terms of H_2-TPR measurements (not shown). Based on such information, the weight loss below 225°C can be ascribed to the removal of adsorbed oxygen species while that beyond 225°C to the removal of lattice oxygen species associated with Co^{3+} as well as Co^{2+} cations (Fig. S2). Therefore, the amount of adsorbed oxygen species can be quantitatively estimated: d-Co_3O_4 (1.16 mmol g_{cat}^{-1} or 5.4 μmol m^{-2}), c-Co_3O_4 (0.06 mmol g_{cat}^{-1} or 7.1 μmol m^{-2}), Au/d-Co_3O_4 (0.81 mmol g_{cat}^{-1} or 6.4 μmol m^{-2}), and Au/c-Co_3O_4 (0.31 mmol g_{cat}^{-1} or 25.2 μmol m^{-2}). On the basis of unit mass of catalyst, the values obtained on d-Co_3O_4 and Au/d-Co_3O_4 are considerably higher than that on c-Co_3O_4 and Au/c-Co_3O_4; while on the basis of unit surface area of catalyst, the values showed an opposite trend. Clearly, the estimated amount of adsorbed oxygen species can in part account for the catalytic behaviours of different samples, but it is not the sole factor that determined the catalytic activities in either conversion rates or TORs (Table 3).

XPS

The results of XPS investigation on the treated and untreated samples are shown in Fig. 7. For the untreated Au/d-Co_3O_4, the BE of Au $4f_{7/2}$ as well as Au $4f_{5/2}$ is 83.9 eV and 87.6 eV, respectively; while for the treated one, the BE is 84.0 eV and 87.7 eV, respectively (Fig. 7a). Although the Au NPs are largely in metallic state according to the corresponding BE values [4], there seemed AuO_x species existing in the untreated Au/d-Co_3O_4 and they were essentially changed into Au^0 entities after pretreatment. Note also that there is little change in the BE of Au^0 entities after in situ pretreatment, and this is different from our previous observation made on the hollow structured Au/FeO_x system where the Au NPs became electronically deficient upon pretreatment [33]. This may explain the reason why comparably small enhancement in CO oxidation activity over the treated Au/d-Co_3O_4 with respect to the treated d-Co_3O_4. The results of O1s signals of the treated and untreated d-Co_3O_4 and Au/d-Co_3O_4 with deconvolution (Fig. 7b) clearly illustrated that after in-situ pretreatment, there appears less amount of oxygen adspecies but increased amount of surface lattice oxygen species on the treated d-Co_3O_4 substrate as well as Au/Co_3O_4 [44,45], coincident with the fact that there are higher fractions of Co^{3+} in the treated samples and the shift in BEs of surface lattice oxygen to lower end.

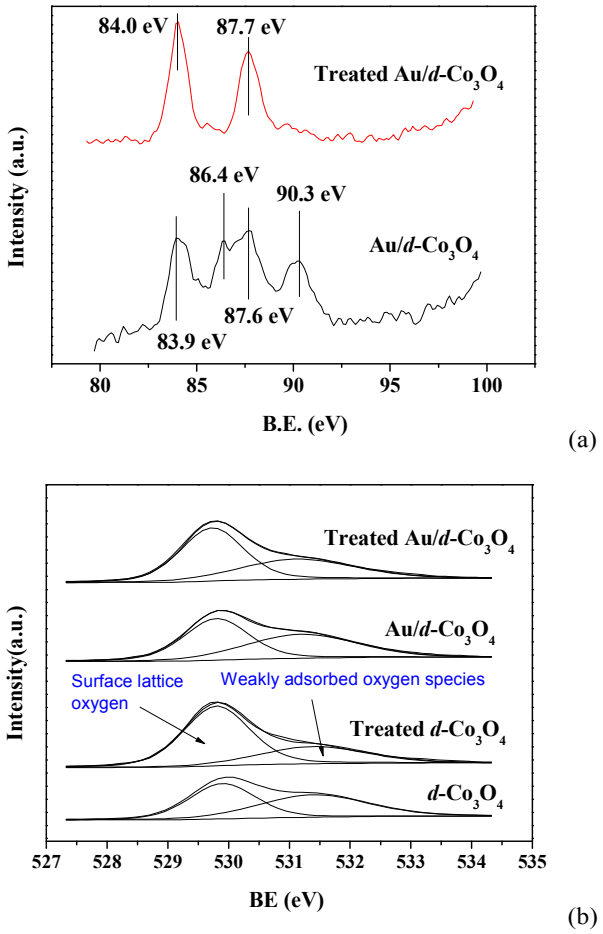

Fig. 7 (a) Au 4f, and (b) O 1s XPS spectra of the treated and untreated d-Co_3O_4 and Au/d-Co_3O_4 nanostructures.

Concerning the oxidation state of the Co cations, one can see that the adopted pretreatment notably increased the Co^{3+} fraction in the treated d-Co_3O_4 (Co^{3+}/Co^{2+} = 5.4 vs. 2.5) while it caused slight change in the Co^{3+} fraction of the treated Au/d-Co_3O_4 (Co^{3+}/Co^{2+} = 4.2 vs. 4.0) (Fig. 8). Clearly, the presence

of Au NPs had an impact on the surface state of Co_3O_4 substrate.

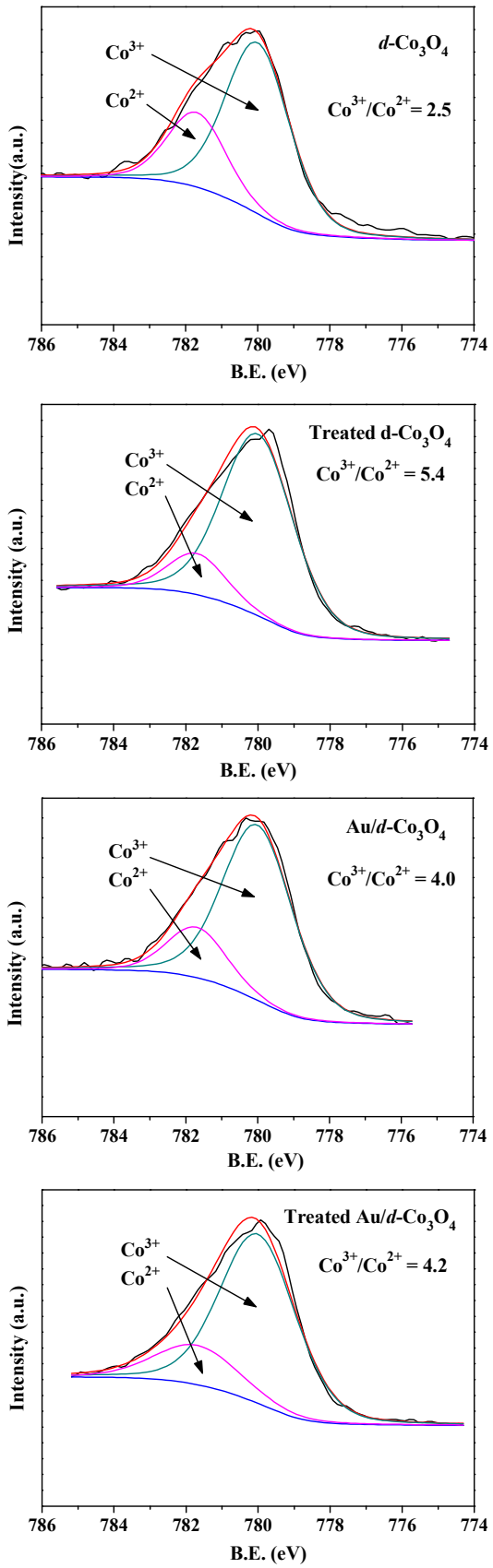

Fig. 8 Deconvolution analysis of the Co 2p XPS peaks of the untreated and treated d-Co_3O_4 and Au/d-Co_3O_4.

Previous studies revealed that the Co^{3+} species are the active sites for CO oxidation [46]. The results of the current work are also coincident well with the early observations: the in-situ pretreated catalysts containing high fraction of surface Co^{3+} showed enhanced activity (see below); and XPS analysis of c-Co_3O_4 which had experienced calcination indicated the surface Co cations were essentially Co^{3+} (not shown), accounting for its reserved activity even if the catalyst had rather small surface area.

Applying the technique of temporal analysis of products (TAP), Widmann et al. [47] demonstrated that the calcined Au/CeO_2 was only slightly active for CO oxidation, and small amount of surface oxygen should be removed before the catalyst reached its more active steady-state surface composition. The activity was notably increased on a catalyst surface with relatively lower surface oxygen concentration, while the over-reduction of surface oxygen coverage would cause lower initial activity. In the present case, although there was small effect on the original Au^0 entities upon in situ pretreatment; the accompanying transformation of AuO_x to Au^0 may enhance competitive CO adsorption on the generated Au^0 entities.

Both O_2-TPD and XPS results of the present study (Figs. 6 and 7) indeed demonstrated that there was relatively low surface concentration of oxygen adspecies on the treated d-Co_3O_4 and Au/d-Co_3O_4. Bear in mind that, the spillover of oxygen adspecies from Au NPs onto the Au-Co_3O_4 boundary region could not only reduce surface oxygen coverage on the Au NPs, but also add extra oxygen anions around the Au-Co_3O_4 boundary where the coming oxygen species would react with the neighboring adsorbed CO to CO_2.

Catalytic activity

There were investigations demonstrating single and mixed transition metal oxides potential for CO oxidation [48,49]. Co_3O_4 was found to be one of the most active oxides toward this reaction [50-52]. However, the activity and stability was found to be highly dependent on sample morphology, and the deposition of Au NPs on the unique Co_3O_4 spheroids for CO oxidation has not been explored yet. Fig. 9 illustrates the CO conversions at elevated temperatures on various catalysts. In view of Fig. 9a, CO oxidation performance was enhanced only when the Au NPs were deposited on the d-Co_3O_4 spheroids. Interestingly, the pretreatment of the catalysts at 180 °C for 2 h in the reaction stream [$CO/O_2/N_2$ = 1.6/21/77.4 (v/v/v)] would significantly enhance catalyst activity (Fig. 9b). According to the values of T_{100} (the temperature at which 100% CO conversion is achieved), both Au/c-Co_3O_4 and Au/d-Co_3O_4 became more active in CO oxidation after in-situ pretreatment, and the T_{100} of the treated Au/d-Co_3O_4 is only 80 °C. It is worth noting that the Co_3O_4 substrates, whether calcined or not, also encountered the in-situ pretreatment effect on CO oxidation, particularly the d-

Co_3O_4 (Fig. 9c). Table 2 summarized the activities of all treated catalysts on the basis of per unit mass of catalyst, and the following activity sequence was obtained based on the T_{100} values: treated Au/d-Co_3O_4 (T_{100} = 80 °C) > treated d-Co_3O_4 (T_{100} = 90 °C) > treated Au/c-Co_3O_4 (T_{100} = 110 °C) > treated c-Co_3O_4 (T_{100} =120 °C) > untreated d-Co_3O_4 (T_{100} = 130 °C). Note that the d-Co_3O_4 associated catalysts generally outperformed the c-Co_3O_4 based counterparts. On the other hand, when the catalyst activities were compared on the basis of per unit surface area of catalyst (TORs), the opposite tendency was observed (Table 3). This implies that although the surface areas of the c-Co_3O_4 based catalysts are rather small, the density of active sites is still sufficiently high for CO oxidation over the c-Co_3O_4 based catalysts.

Table 2 Temperatures at CO complete conversion over various Co_3O_4-based catalysts subjected to in situ pretreatment

Catalysts-calcined	*c*-Co_3O_4	Au/*c*-Co_3O_4
T_{100}/°C	130	110
Catalysts-dried	*d*-Co_3O_4	Au/*d*-Co_3O_4
T_{100}/°C	90	80

In the case of Au/d-Co_3O_4, the Au particle size is comparably small (ca. 2 nm), and with decreasing Au particle size, the electronic property of Au NPs deviate somewhat from bulk Au [11]. However, the Co_3O_4 substrate is non-inert and can modify the electronic state of Au NPs especially when a strong Au-Co_3O_4 interaction exists. That should be true for both Au/d-Co_3O_4 and Au/c-Co_3O_4, since in the former the very fine Au NPs can be confined in the fine pores of d-Co_3O_4 while in the latter the flat Au entities can tightly contact with the condensed surfaces of c-Co_3O_4. Note also that it is hard to say the metallic Au is always more active than AuO_x species, since the activity of the latter species is rather dependent upon the oxygen stoichiometry in AuO_x. In the current study, there seems AuO_x species with high oxygen content (i.e. high oxidation state of $Au^{\delta+}$) in the untreated Au/d-Co_3O_4, accounting for its comparatively poor activity.

Table 3 CO conversion rates and TOPs over various treated catalysts at 80°C

Sample	**CO conversion rate** $\mu mol\ g^{-1}\ min^{-1}$	**TOR** $\mu mol\ m^{-2}\ min^{-1}$
treated *c*-Co_3O_4	31.4	3.7
treated *d*-Co_3O_4	191.4	0.9
treated Au/*c*-Co_3O_4	23.2	1.9
treated Au/*d*-Co_3O_4	222.8	1.8

Liu et al. synthesized the ordered mesoporous Co_3O_4 supported Au nanocatalysts for CO and VOCs combustion [53]. According to the T_{100} values, the d-Co_3O_4 of this study was nearly as active as the ordered mesoporous Co_3O_4 substrate under the comparable conditions. The mesoporous Co_3O_4 supported Au NPs seemed remarkably active for CO oxidation, although the Au particle size distribution in Au/mesoporous Co_3O_4 looked similar to that of Au/d-Co_3O_4. The method used for Au introduction, however, was different in the two studies. In the present case, the Au introduction was achieved via the DP process, while in the case of Au/mesoporous Co_3O_4, the Au introduction was established via chemical reduction of $HAuCl_4$ with $NaBH_4$ and adsorption of Au colloid particles. Therefore, the nature of Co_3O_4 substrate (even in the same chemical constitution) as well as the Au NPs and the involved Au-Co_3O_4 interaction, which are greatly influenced by preparation history, should account for the difference in activity of these Au/Co_3O_4 systems. Li et al. [54] reported CO oxidation over the iodine-ion-induced size-tunable Co_3O_4 nanowires. This catalyst system was highly efficient by employing extraordinarily high value of GHSV, but it became almost inactive below 100 °C and deactivated over time below 120°C. In addition, the very reactive Au-containing catalysts generally suffer poor durability of catalyst [21].

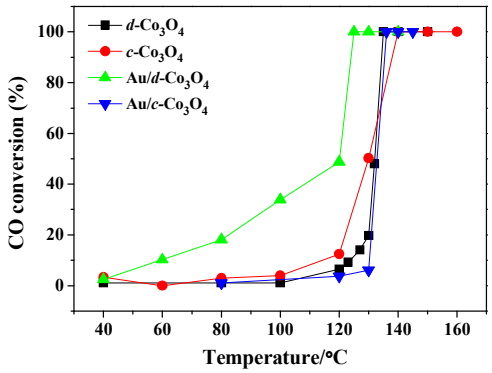

(a)

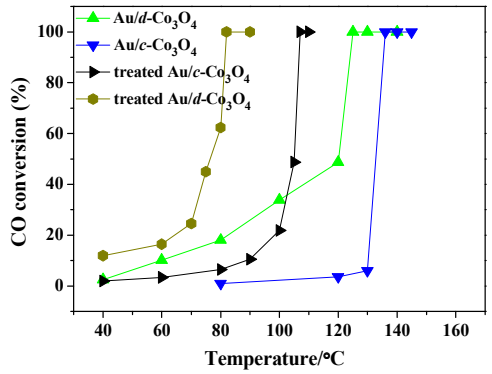

(b)

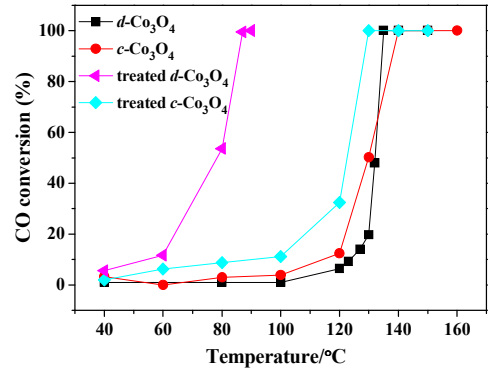

(c)

Fig. 9 Temperature dependence of CO conversions over various catalysts without/with in situ pretreatment.

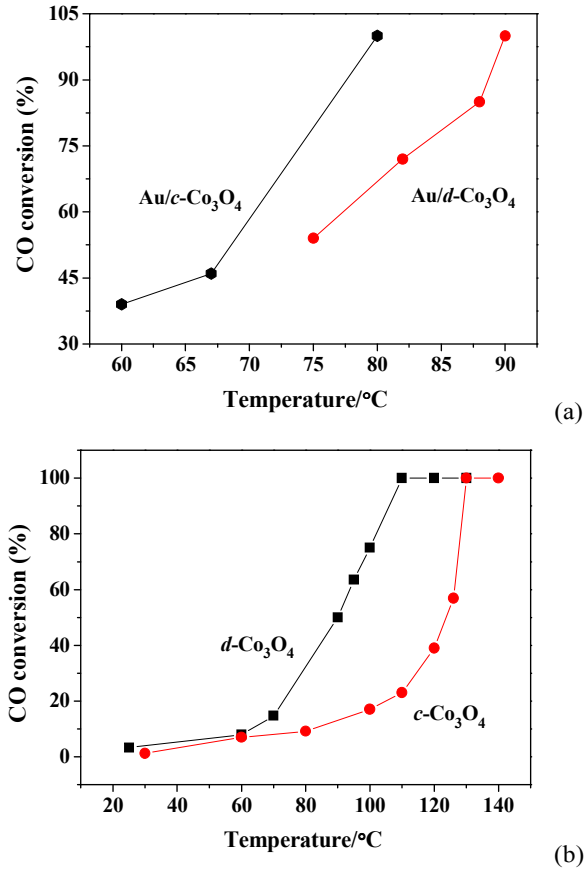

Fig. 10 Temperature dependence of CO conversion on (a) Au/c-Co_3O_4 and Au/d-Co_3O_4 and (b) c-Co_3O_4 and d-Co_3O_4: all of the samples had been subjected to pre-reaction at 350 °C for 5 h.

In the current study, when Au/c-Co_3O_4 and Au/d-Co_3O_4 first experienced CO oxidation at 350 °C for 5 h, and then were operated at temperatures of 50-90 °C, the former can obviously outperform the latter (Fig. 10a), although the corresponding substrates still showed a reverse order (Fig. 10b). This indicated that Au/c-Co_3O_4 is more competent to a high-temperature environment, and the stability tests over Au/c-Co_3O_4 and Au/d-Co_3O_4 within a period of 350-650 min further confirmed this point (Fig. S4). Clearly, Au aggregation is more evident in Au/d-Co_3O_4 (Fig. 1a vs. Fig. S3a) than Au/c-Co_3O_4 (Fig. 1b vs. Fig. S3b). In addition, the former is notably less durable than the latter after pre-reaction at 350 °C for 5 h (Fig. S4). We also tested several yolk-shell type Co_3O_4@SiO_2 catalysts by controllable acid-etching of Co_3O_4 cores, in contrast to those prepared by employing the acid-etching of auxiliary shells [15,39,55]. The measured T_{100} values obtained on the catalysts of non-acid-etched Co_3O_4@SiO_2, slightly acid-etched Co_3O_4@SiO_2, and moderately acid-etched Co_3O_4@SiO_2 are 157 °C, 100 °C, and 130 °C respectively. The acid-treatment did dissolve portion of the cobalt oxide, especially at the SiO_2-Co_3O_4 boundary, releasing some free surfaces of Co_3O_4, meanwhile modifying the surface morphology of Co_3O_4 cores. By changing the condition of acid-treatment, the degree of acid-etching of the core-shell catalyst can be controlled, resulting in different sized Co_3O_4 cores and certain Co_3O_4-SiO_2 contact. As indicated, only the slightly acid-etched catalyst showed favourable Co_3O_4 core size and optimal Co_3O_4-SiO_2 contact for the reaction. Even when operated at a rather high temperature, these Co_3O_4-based core-shell catalysts showed their superb stability because of the protective SiO_2 shells. Note that there is micro-/meso-porosity in SiO_2 shells reflected by big differences in the BET surface area and pore volume between Co_3O_4 and Co_3O_4@SiO_2 (Table 1), which allows effective acid-etching of Co_3O_4 cores through the pores of SiO_2 layers. Moreover, our previous studies have indicated that there is no mass transportation limitation for catalytic NH_3 decomposition, CH_4 partial oxidation, and CO oxidation on a variety of core-shell structured M@SiO_2 (M = Fe, Co, Ni, and Ru) [37b-g] where the SiO_2 encapsulation was achieved by employing the essentially identical synthetic approach as in the current study.

For CO oxidation over the Co_3O_4 nanostructures of different morphologies [56], the specifically prepared Co_3O_4 nanorods were found to be exceptionally active. Nie et al. [57] recently reported that oxygen pretreatment of $Au_{25}(SR)_{18}$ nanoclusters supported on CeO_2, TiO_2, and Fe_2O_3 oxides at 150 °C resulted in a notable enhancement in the CO oxidation activities. The same phenomenon was also reported by us on the hollow structured Au/FeO_x [40] and the Co_3O_4 and Au/Co_3O_4 of the present study. It is considered that there are parallel reaction pathways for CO oxidation over the catalyst surfaces: one is over the Au NPs, another is over the Co_3O_4 substrate, while the third is at the Au-Co_3O_4 interfaces, as previously observed by Haruta et al. [6], Santos et al. [58], Solsona et al. [59], and us [60]. Note that all of the catalysts (even for d-Co_3O_4) were quite stable when they were operated in the 60-130 °C temperature range for a reaction period beyond 70 h. If a catalyst was subjected to a 350 °C-reaction, then only Au/c-Co_3O_4 could reserve reasonably high activity; and if a catalyst experienced a high-temperature process beyond 350 °C, then only the core-shell structured Co_3O_4@SiO_2 catalyst retained good durability.

In the present study, we made the comparative study on the Co_3O_4 substrates with/without Au deposition. It was found that the effect of Au deposition was determined by not only type of oxide substrate but also preparation history and characteristics of Co_3O_4 substrate itself. The presence of Au did modify the physic-chemical properties of the Co_3O_4 substrates (for instances the surface oxidation state, the adsorption/desorption as well as reduction behaviours of oxygen species etc., as revealed by the investigations of XPS, O_2-TPD, and H_2-TPR). The nature of Co_3O_4 substrate in turn strongly influenced the Au-dispersion and Au-Co_3O_4 interaction. The effectiveness in activity and particularly durability of Au species on the target Co_3O_4 substrate has been revealed, which is meaningful for developing highly durable Au-containing catalysts for different applications.

Conclusions

Spherically shaped Co_3O_4 particles were synthesized by one-pot solvothermal process free of structure directing agent or pore former. The dried Co_3O_4 spheroids processed rich of fine pores in which very small sized Au NPs (ca. 2 nm) were confined in the micropores of dried Co_3O_4, active (T_{100} = 80-90 °C) and very stable (TOS > 70 h) for CO oxidation. Upon calcination, there were condensed Co_3O_4 spheroids formed on which small sized flat Au entities (3.0 ± 0.6 nm) with remarkably large Au-Co_3O_4 interfaces were uniformly dispersed, outperforming Au/d-Co_3O_4 in both activity and stability even after experienced a pre-reaction at 350°C for 5 h. As for the yolk-shell type Co_3O_4@SiO_2 catalysts synthesized by controllable acid-etching of Co_3O_4 cores, there were an optimal Co_3O_4 core-SiO_2 shell interaction and also appropriate Co_3O_4 core particle size for CO oxidation. The Au/c-Co_3O_4 and Au/c-Co_3O_4@SiO_2 catalysts were substantially durable even at temperatures ≥ 350 °C, due to the intensive Au-Co_3O_4 interaction in Au/c-Co_3O_4 or the effective protection of SiO_2 shells in Au/c-Co_3O_4@SiO_2. The Co_3O_4 spheroids as well as their supported Au NPs encountered the in-situ pretreatment enhanced CO oxidation, as previously observed on the hollow structured Au/FeO_x by us. The pretreatment resulted in: (i) transformation of AuO_x to Au^0, (ii) higher fraction of surface Co^{3+}, and (iii) suitably lower concentration of surface oxygen adspecies, accounting for the enhanced activities of CO oxidation.

Acknowledgements

We greatly appreciated the financial support from NSFC (21173118), NSFJS (BK2011439), MSTC (2013AA031703), and MOE (20110091110023).

Notes and references

[a] Key Laboratory of Mesoscopic Chemistry, MOE, School of Chemistry and Chemical Engineering, Nanjing University, 22 Hankou Road, Nanjing 210093, China. Fax: +86-25-83317761; Tel: +86-25-83686270; E-mail: jiwj@nju.edu.cn.

[b] Nanjing University-Yangzhou Institute of Chemistry and Chemical Engineering, Yangzhou 211400, China.

[c] Department of Chemistry, Hong Kong Baptist University, Hong Kong, China, Fax: +852-34117348; E-mail: pctau@hkbu.edu.hk

† Electronic supplementary information (ESI) available: HRTEM iamges of Au/c-Co_3O_4 (used); TGA profiles of d-Co_3O_4, c-Co_3O_4, Au/d-Co_3O_4, and Au/c-Co_3O_4 in reducing atmosphere (5%H_2-Ar); TEM images of Au/c-Co_3O_4 and Au/d-Co_3O_4 after pre-reaction at 350 °C for 5 h; and stability tests over Au/c-Co_3O_4 and Au/d-Co_3O_4 after pre-reaction at 350 °C for 5 h

1 M. V. Twigg, *Appl. Catal. B.*, 2007, **70**, 2.
2 X. W. Xie, Y. Li, Z. Q. Liu, M. Haruta and W. J. Shen, *Nature*, 2009, **458**, 746.
3 G. J. Hutchings, *J. Catal.*, 1985, **96**, 292.
4 M. Date, M. Okumura, S. Tsubota and M. Haruta, *Angew. Chem. Int. Ed.*, 2004, **43**, 2129.
5 M. Haruta, T. Kobayashi, H. Sano and N. Yamada, *Chem. Lett.*, 1987, **16**, 405.
6 M. Haruta, S. Tsubota, T. Kobayashi, H. Kageyama, M. J. Genet and B. Delmon, *J. Catal.*, 1993,**144**, 175.
7 a) M. Haruta, N. Yamada, T. Kobayashi and S. Iijima, *J. Catal.*, 1989, **115**, 301. b) G. J. Hutchings and M. Haruta, *Appl. Catal. A: Gen.*, 2005, **291**, 2.
8 H. H. Kung, M. C. Kung and C. K. Costello, *J. Catal.*, 2003, **216,** 425.
9 S. Royer and D. Duprez, *ChemCatChem*, 2011, **3**, 24.
10 Z. Z. Wei, D. C. Li, X. Y. Pang, C. Q. Lv and G. C. Wang, *ChemCatChem*, 2012, **4**, 100.
11 K. Qian, L. F. Luo, H. Z. Bao, Q. Hua, Z. Q. Jiang and W. X. Huang, *Catal. Sci. Technol.*, 2013, **3**, 679.
12 Z. P. Hao, L. D. An, J. L. Zhou and H. L.Wang, *Catal. Lett.*, 1996, **59**, 295.
13 Z. P. Hao, D. Y. Cheng, Y. Guo and Y. H. Liang, *Appl. Catal. B.*, 2001, **33**, 217.
14 J. J. Li, C. Y. Ma, X. Y. Xu, J. J. Yu, Z. P. Hao and S. Z. Qiao, *Environ. Sci. Technol.*, 2008, **42**, 8947.
15 C. Y. Ma, Z. Mu, J. J. Li, Y. G. J, J. Cheng, G. Q. Lu, Z. P. Hao and S. Z. Qiao, *J. Am. Chem. Soc.*, 2010, **132,** 2608.
16 H. Y. Lin and Y. W. Chen, *Ind. Eng. Chem. Res.*, 2005, **44**, 4569.
17 J. Sa, S. F. R. Taylor, H. Daly, A. Goguet, R. Tiruvalam, Q. He, C. J. Kiely, G. J. Hutchings and C. Hardacre, *ACS Catal.*, 2012, **2**, 552.
18 G. R. Zhang, D. Zhao, Y. Y. Feng, B. S. Zhang, D. S. Su, G. Liu and B. Q. Xu, *ACS Nano.*, 2012, **6**, 2226.
19 L. F. Liotta, H. J. Wu, G. Pantaleoa and A. M. Venezia, *Catal. Sci. Technol.*, 2013, **3**, 3085.
20 Y. Y. Yao, *J. Catal.*, 1974, **33**, 108.
21 R. S. Drago, K. Jurczyk, D. J. Singh and V. Young, *Appl. Catal. B.*, 1995, **6**, 155.
22 J. Li, G. Z. Lu, G. S. Wu, D. S. Mao, Y. L. Guo, Y. Q. Wang and Y. Guo, *Catal. Sci. Technol.*, 2014, **4**, 1268.
23 P. M. Kouotou, H. Vieker, Z. Y. Tian, P. H. T. Ngamou, A. El Kasmi, A. Beyer, A. Gölzhäuserb and K. Kohse-Höinghausa, *Catal. Sci. Technol.*, 2014, **4**, 3359.
24 R. A. Pai, R. Humayun, M. T. Schulberg, A. Sengupta, J. N. Sun and J. J. Watkins, *Science*, 2004, **303**, 507.
25 H. G. Yang, G. Liu, S. Z. Qiao, C. H. Sun, Y. G. Jin, S. C. Smith, J. Zou, H. M. Cheng and G. Q. Lu, *J. Am. Chem. Soc.*, 2009, **131**, 4078.
26 L. H. Hu, K. Q. Sun, Q. Peng, B. Q. Xu and Y. Li, *Nano Res.*, 2010, **3**, 363.
27 C. Xu, Y. Liu, C. Zhou, L. Wang, H. Geng and Y. Ding, *ChemCatChem*, 2011, **3**, 399.
28 Y. Sun, P. Lv, J. Y. Yang, L. He, J. C. Nie, X. Liu and Y. Li, *Chem. Commun.*, **2**011, **47**, 11279.
29 Y. Teng, Y. Kusano, M. Azuma, M. Haruta and Y. Shimakawa, *Catal. Sci. Technol.*, 2011, **1**, 920.
30 H. F. Wang, R. Kavanagh, Y. L. Guo, Y. Guo, G. Lu and P. Hu, *J. Catal.*, 2012, **296**, 110.
31 L. Hu, Q. Peng and Y. Li, *J. Am. Chem. Soc.*, 2008, **130**, 16136.
32 C. Bae, H. Yoo, S. Kim, K. Lee, J. Kim, M. A. Sung and H. Shin, *Chem. Mater.*, 2008, **20**, 756.
33 Z. Y. Fei, S. C. He, L. Li, W. J. Ji and C. T. Au, *Chem. Commun.*, 2012, **48**, 853.

34 B. Sun, X. Z. Feng, Y. Yao, Q. Su, W. J. Ji and C. T. Au, *ACS Catal*., 2013, **3**, 3099.
35 a) M. Danek, K. F. Jensen, C. B. Murray and M. G. Bawendi, *Chem. Mater*., 1996, 8, 173. b) V. Skumryev, S. Stoyanov, Y. Zhang, G. Hadjipanayis, D. Givord and J. Nogues, *Nature*, 2003, **423**, 850.
36 a) T. Mitsudome and K. Kaneda, *ChemCatChem*, 2013, **5**, 1681. b) J. Kim, J. E. Lee, J. Lee, J. H. Yu, B. C. Kim, K. An, Y. Hwang, C. H. Shin, J. G. Park, J. Kim and T. Hyeon, J. *Am. Chem. Soc*., 2006, **128**, 688. c) S. Giri, B. G. Trewyn, M. P. Stellmaker and V. S. Y. Lin, *Angew. Chem., Int. Ed*., 2005, **44**, 5038.
37 a) B. Zeng, B. Hou, L. T. Jia, J. G. Wang, C. B. Chen, D. B. Li and Y. H. Sun, *Catal. Sci. Technol.*, 2013, **3**, 3250. b) Y. X. Li, S. Q. Liu, L. H. Yao, W. J.Ji and C. T. Au, *Catal. Commun.*, 2010, **11**, 368. c) L. H. Yao, T. B. Shi, Y. X. Li, J. Zhao, W. J. Ji and C. T. Au, *Catal. Today*, 2011, **164**, 112. d) Y. X. Li, L. H. Yao, Y. Y. Song, S. Q. Liu, J. Zhao, W. J. Ji and C. T. Au, *Chem. Commun.*, 2010, **46**, 5298. e) L. Li, S. C. He, Y. Y. Song, J. Zhao, W. J. Ji and C. T. Au, *J. Catal.*, 2012, **288**, 54. f) L. Li, Y. Yao, B. Sun, Z. Y. Fei, J. Zhao, W. J. Ji and C. T. Au, *ChemCatChem*, 2013, **5**, 3781. g) S. C. He, Z. Y. Fei, L. Li, B. Sun, X. Z. Feng and W. J. Ji, *Chin. J. Catal.*, 2013, **34**, 2098.
38 Y. H. Deng, D. W. Qi, C. H. Deng, X. M. Zhang and D. Y. Zhao, *J. Am. Chem. Soc*., 2008, **130**, 28.
39 W. Li, Y. H. Deng, Z. X. Wu, X. F. Qian, J. P. Yang, Y. Wang, D. Gu, F. Zhang, B. Tu and D. Y. Zhao, *J. Am. Chem. Soc*., 2011, **133**, 15830.
40 R. Y. Xie, D. B. Li, B. Hou, J. G. Wang, L. T. Jia and Y. H. Sun, *Catal. Commun*., 2011, **12**, 380.
41 G. Pattrick, E. van der Lingen, C. W. Corti, R. J. Holliday and D. T. Thompson, *Top. Catal*., 2004, **30-31**, 273.
42 X. Wang, X. Y. Chen, L. S. Gao, H. G. Zheng, Z. D. Zhang and Y. T. Qian, *J. Phys. Chem. B*., 2004, **108**, 16401.
43 L. Xue, C. B. Zhang, H. He and Y. Teraoka, *Appl. Catal. B.*, 2007, **75**, 167.
44 J. L. Cao, Y. Wang, X. L. Yu, S. R. Wang, S. H. Wu, and Z. Y. Yuan, *Appl. Catal. B-Enviro.*, 2008, **79**, 26.
45 J. C. Dupin, D. Gonbeau, P. Vinatier and A. Levasseur, *Phys. Chem. Chem. Phys.*, 2000, **2**, 1319.
46 a) J. Jansson, A. E. C. Palmqvist, E. Fridell, M. Skoglundh, L. Österlund, P. Thormählen and V. Langer, *J. Catal.*, 2002, **211,** 387. b) F. Grillo, M. M. Natile, and A. Glisenti, *Appl. Catal. B: Environ.*, 2004, **48**, 267. c) Y. Gou, X. Liang, and B. H. Chen, *J. Alloys Compounds*, 2013, **574**, 181.
47 D. Widmann, R. Leppelt and R. J. Behm, *J. Catal.*, 2007, **251**, 437.
48 J. W. Saalfrank and W. F. Maier, *Angew. Chem.*, 2004, **116**, 2062.
49 C. B. Wang, C. W. Tang, H. C. Tsai and S. H. Chien, *Catal. Lett*., 2006, **107**, 223.
50 D. Berger, F. Morfin, C. Matei, J.C. Volta and J. Optoelectron, *Adv. Mater*., 2007, **9**, 1540.
51 a) Y. J. Mergler, J. Hoebink and B. E. Nieuwenhuys, *J. Catal.*, 1997, **167**, 305. b) J. Jansson, M. Skoglundh, E. Fridell and P. Thormählen, *Top. Catal*., 2001, **16-17**, 385.
52 G. Salek, P. Alphonse, P. Dufour, S. Guillemet-Fritsch and C. Tenailleau, *Appl. Catal. B.*, 2014, **147**, 1.
53 Y. X. Liu, H. X. Dai, J. G. Deng, S. H. Xie, H. G. Yang, W. Tan, W. Han, Y. Jiang and G. S. Guo, *J. Catal.*, 2014, **309**, 408.
54 Y. G. Li, L. P. Zhu, Y. M. Guo, J. Jiang, L. Hu, Z. Wen, L. W. Sun and Z. Z. Ye, *ChemCatChem*, 2013, **5**, 3576.
55 C. H. Kuo, Y. Tang, L.Y. Chou, B. T. Sneed, C. N. Brodsky, Z. P. Zhao and C. K. Tsung, *J. Am. Chem. Soc.*, 2009, **13**1, 2774.
56 D. A. H. Cunningham, T. Kobayashi, N. Kamijo and M. Haruta, *Catal. Lett*., 1994, **25**, 257.
57 X.T. Nie, H. F. Qian, Q. J. Ge, H. Y. Xu and R. C. Jin, *ACS Nano*., 2012, **6**, 6014.
58 V. P. Santos, M. F. R. Pereira, J. J. M. Órfao and J. L. Figueiredo, *Appl. Catal. B.*, 2010, **99**, 353.
59 B. Solsona, T. E. Davies, T. Garcia, I. Vazquez, A. Dejoz and S. H. Taylor, *Appl. Catal. B.*, 2008, **84**, 176.
60 Z. Y. Fei, B. Sun, L. Zhao, W. J. Ji and C. T. Au, *Chem. Eur. J.*, 2013, **19**, 6480.